A LuGre Tire Friction Model with Exact Aggregate Dynamics

PANAGIOTIS TSIOTRAS*†, EFSTATHIOS VELENIS*
and MICHEL SORINE‡

SUMMARY

The LuGre dynamic point contact friction model for the two-dimensional translation of a body on a surface has been used to derive a model for the friction forces and moments at the contact patch of a tire. The resulting tire friction model is distributed, i.e., is described by a set of partial differential equations. Several approximations have been used in the literature to approximate this distributed model using a set of ordinary differential equations, making the model more appropriate for control design and on-line estimation. In this paper the method of moments is used to derive a set of ordinary differential equations to describe the exact average dynamics of the distributed model. Three cases of normal load distribution are considered and compared with each other: uniform, trapezoidal and quartic load distribution. Simulations are also presented to compare with existing approximate lumped models.

1 INTRODUCTION

In the past several years, the problem of modeling and predicting tire friction has become an area of intense research in the automotive community. Knowledge of the friction characteristics is necessary for the development of control systems such as ABS, TCS, ESP, etc. which have enhanced safety and maneuverability of modern passenger vehicles.

Recently, a new class of tire friction models has been developed that captures the dynamic behavior of friction forces–the so-called "dynamic tire friction models." In [1] dynamic models that handle the rate-independent hysteresis phenomena observed in practice were proposed. As an application to this work, a dynamic elastoplastic friction model was developed in [2]. This friction model

*School of Aerospace Engineering, Georgia Institute of Technology, Atlanta, GA 30332-0150, USA, Tel: +1-404-894-9526, Fax: +1-404-894-2760, Email:{p.tsiotras, efstathios_velenis}@ae.gatech.edu

†Corresponding author.

‡INRIA Rocquencourt, Domaine de Voluceau, B.P. 105, 78153 Le Chesnay Cedex, FRANCE, Tel: +33-1-39635648, Fax: +33-1-39635786, Email:michel.sorine@inria.fr

was then applied to the longitudinal motion of a tire in [3] and extended to the longitudinal/lateral motion in [4, 5].

The longitudinal LuGre tire friction model, initially introduced in [6] and later corrected and improved upon in [7, 8], is based on a dynamic visco-elastoplastic friction model for point contact introduced in [9]. These results were later extended to the combined longitudinal/lateral motion in [10, 11]. In [12] the LuGre tire friction model for combined longitudinal/lateral motion was further refined by taking into account all aspects neglected in [10, 11], that is, coupling of the forces in longitudinal and lateral directions (neglected in [10]), tire anisotropy (neglected in [11]) and rim rotation (neglected in both [10] and [11]). In addition, a solid mathematical justification for the introduction of dynamic friction models based on fundamental physical properties of the friction forces (such as dissipativity and maximality of the dissipation rate) as in [13], was provided.

The major advantage of the LuGre dynamic tire friction model, when compared to the one in [4, 5], is its simpler lumped form. The term *lumped form* refers to the model's description by a set of ordinary differential equations. Both models in [4, 5] as well as the LuGre tire friction model were initially derived as distributed models described by a set of partial differential equations. The lumped model in [4, 5] was derived using a finite element approach, resulting in a system with a potentially large number of states. In [10, 11, 12] the lumped LuGre tire model was derived by introducing the mean states along the length of the contact patch. Its behavior can be described by a system of three ordinary differential equations. These equations give the forces and the aligning moment at the contact patch of the tire.

A lumped form makes the model more suitable for the development and implementation of on-line estimation and control algorithms [14, 15, 16]. The main objective of the lumped model in [10, 11, 12] was to be able to capture the steady-state behavior of the distributed model exactly. Therefore, this model does not offer any guarantees on the accuracy of the transient dynamics.

In this paper, the derivation of the lumped LuGre tire model is revisited, this time using the method of moments formulation [17]. The method of moments is commonly used to describe the overall behavior of distributed systems. It has been used successfully in many applications [18, 19]. Herein we derive an average lumped model that captures the exact dynamics of the distributed model. This allows one to validate the assumptions used in the literature for the derivation of simpler, low order lumped models.

In the first section of this paper the distributed LuGre tire model is reviewed. Next, the essential definitions of the method of moments are provided and the exact lumped model is derived for three specific cases of normal load distribution, namely, uniform, trapezoidal and quartic distribution. At the end of the paper numerical simulations are presented to compare the dynamic behavior of the simplified low order lumped models of [10, 11, 12] with the aggregate dynamics of the distributed model.

2 THE DISTRIBUTED LUGRE DYNAMIC TIRE FRICTION MODEL

The distributed LuGre tire friction model for combined longitudinal/lateral motion was derived in [12] by applying the point contact LuGre friction model (for the two-dimensional translation of a body on a surface) on the contact patch of a tire. In order to take into consideration the fact that undeformed tire elements enter the contact patch as the tire rotates, the contact patch was divided into infinitesimal stripes $\mathrm{d}\zeta$ along the length of the contact patch (Fig. 1). The point contact model was then applied to the tire elements at each of the infinitesimal stripes thus resulting in a model described by a set of partial differential equations, with time t and longitudinal position on the patch ζ being the independent variables.

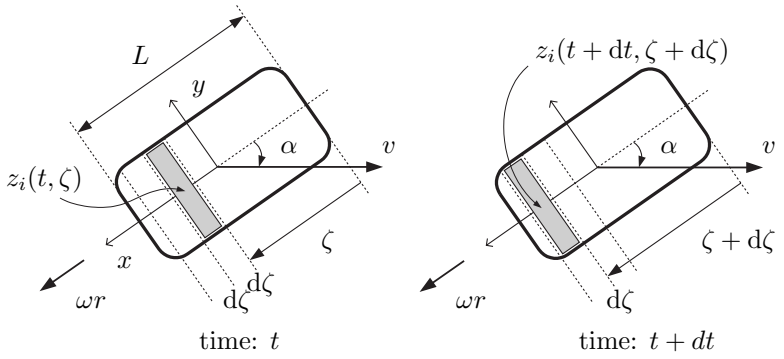

Figure 1: Frame of reference and velocities at the contact patch. Derivation of the distributed tire model.

The distributed tire model is summarized in the following equations [12]

$$\begin{aligned}
\frac{\mathrm{d}z_i(t,\zeta)}{\mathrm{d}t} &= \frac{\partial z_i(t,\zeta)}{\partial t} + |\omega r|\frac{\partial z_i(t,\zeta)}{\partial \zeta} \\
&= v_{ri}(t) - C_{0i}(v_r)z_i(t,\zeta), \qquad i=x,y \qquad (1)\\
\mu_i(t,\zeta) &= -\sigma_{0i}z_i(t,\zeta) - \sigma_{1i}\frac{\partial z_i(t,\zeta)}{\partial t} - \sigma_2 v_{ri}(t), \quad i=x,y \qquad (2)\\
F_i(t) &= \int_0^L \mu_i(t,\zeta)f_n(\zeta)\mathrm{d}\zeta, \quad i=x,y \qquad (3)\\
M_z(t) &= -\int_0^L \mu_y(t,\zeta)f_n(\zeta)\left(\frac{L}{2}-\zeta\right)\mathrm{d}\zeta \qquad (4)
\end{aligned}$$

By $z_i(t,\zeta),\ i=x,y$, we denote the internal friction states [12] which correspond to the elastic deformations of the tire element at time t and position ζ on the contact patch, along the longitudinal x and lateral y directions. In accordance to the above discussion, the boundary condition for equations (1) is $z_i(t,0)=0$.

This imposes the condition that the tire fiber is undeflected as it enters the patch. The constants $\sigma_{0i},\ i = x, y$, correspond to the stiffness of the tire elements in the x and y directions, while σ_{1i} and σ_{2i} are damping constants for the friction coefficient $\mu_i(t, \zeta)$. The functions $C_{0i}(v_r)$ characterize the steady-state characteristics of the model (for more details the reader is referred to [12]). For a tire with the same static friction characteristics along the longitudinal and lateral directions, as the one considered in [11], $C_{0i}(v_r)$ is given by

$$C_{0i}(v_r) = \frac{|v_r|\sigma_{0i}}{g(v_r)}\ , \quad i = x, y \tag{5}$$

where,

$$g(v_r) = \mu_k + \big(\mu_s - \mu_k\big)e^{-\left(\frac{|v_r|}{v_s}\right)^{\gamma}}. \tag{6}$$

In (6) μ_k and μ_s denote the kinetic and static Coulomb friction coefficients, respectively, and v_s denotes the Stribeck characteristic velocity [9]. The parameter γ is used to achieve desirable steady-state behavior of the tire friction [8]. The function $f_n(\zeta)$ in (3) denotes the normal load distribution along the contact patch. The relative velocity components of the contact patch with respect to the road $v_{ri},\ i = x, y$, appear as inputs in the system of equations (1)-(4) and are given by

$$v_{rx} = \omega r - v\cos(\alpha) \tag{7}$$

$$v_{ry} = -v\sin(\alpha) \tag{8}$$

where ω is the angular rate of the tire and r its radius. By v we denote the magnitude of the translational speed of the wheel and by α the slip angle (Fig. 1). The relative velocity vector between the tire and the surface is $v_r = [v_{rx},\, v_{ry}]^T$ and $|v_r| = \sqrt{v_{rx}^2 + v_{ry}^2}$. The output of the model is the longitudinal $F_x(t)$ and lateral $F_y(t)$ friction forces at the center of the patch as well as the aligning moment $M_z(t)$.

In the following sections we present a methodology for expressing the *exact* dynamics of the distributed model (1)-(4) by a set of ordinary differential equations instead of the partial differential equation (1), for several special cases of the normal load distribution $f_n(\zeta)$.

3 EXACT LUMPED MODEL USING THE METHOD OF MOMENTS

Define the pth moment of $z_i(t, \zeta)$ for $\zeta \in [a,\, b]$ as follows

$$M_{p,i}^{ab}(t) := \int_a^b z_i(t, \zeta)\zeta^p \mathrm{d}\zeta, \quad i = x, y \tag{9}$$

Taking the time derivative of $M_{p,i}^{ab}$ yields,

$$\begin{aligned}
\dot{M}_{p,i}^{ab}(t) &= \int_a^b \frac{\partial z_i(t,\zeta)}{\partial t}\zeta^p \mathrm{d}\zeta \\
&= \int_a^b \left(v_{ri} - C_{0i}(v_r) z_i(t,\zeta) - |\omega r| \frac{\partial z_i(t,\zeta)}{\partial \zeta} \right) \zeta^p \mathrm{d}\zeta \\
&= \frac{b^{p+1} - a^{p+1}}{p+1} v_{ri} - C_{0i}(v_r) \int_a^b z_i(t,\zeta)\zeta^p \mathrm{d}\zeta \\
&\quad - |\omega r| \int_a^b \frac{\partial z_i(t,\zeta)}{\partial \zeta}\zeta^p \mathrm{d}\zeta. \qquad (10)
\end{aligned}$$

Integrating by parts, (10) gives a recursive formula for the calculation of all moments $M_{p,i}^{ab}$ for $p \geq 1$

$$\begin{aligned}
\dot{M}_{p,i}^{ab} &= \frac{b^{p+1} - a^{p+1}}{p+1} v_{ri} - C_{0i}(v_r) M_{p,i}^{ab} - |\omega r| z_i(t,\zeta)\zeta^p \Big|_a^b \\
&\quad + |\omega r| p M_{p-1,i}^{ab} \qquad (11)
\end{aligned}$$

For $p = 0$ equation (10) yields

$$\dot{M}_{0,i}^{ab} = (b-a)v_{ri} - C_{0i}(v_r) M_{0,i}^{ab} - |\omega r| \Big(z_i(t,b) - z_i(t,a) \Big) \qquad (12)$$

Given any sufficiently smooth normal load distribution $f_n(\zeta)$, we can approximate f_n with its Taylor series expansion as follows

$$f_n(\zeta) \simeq \sum_{k=0}^{m} c_k \zeta^k \qquad (13)$$

for some constants $c_0, c_1, ..., c_m$. Note that the total normal load on the contact patch is given by

$$F_n = \int_0^L f_n(\zeta) \mathrm{d}\zeta. \qquad (14)$$

Using the definition of the moments $M_{p,i}^{ab}$, and using (13) the friction forces $F_i(t),\ i = x, y$ in (3) can then be written as follows

$$\begin{aligned}
F_i(t) &= -\int_0^L \left(\sigma_{0i} z_i + \sigma_{1i} \frac{\partial z_i}{\partial t} + \sigma_{2i} v_{ri} \right) f_n(\zeta) \mathrm{d}\zeta \\
&= -\sigma_{0i} \sum_{k=0}^{m} c_k M_{k,i}^{0L} - \sigma_{1i} \sum_{k=0}^{m} c_k \dot{M}_{k,i}^{0L} - \sigma_{2i} v_{ri} F_n \qquad (15)
\end{aligned}$$

Finally, the aligning torque $M_z(t)$ in (4) can be written in terms of the moments $M_{p,i}^{ab}$ as

$$M_z(t) = -\int_0^L \left(\sigma_{0y} z_y + \sigma_{1y} \frac{\partial z_y}{\partial t} + \sigma_{2y} v_{ry} \right) f_n(\zeta) \left(\frac{L}{2} - \zeta \right) \mathrm{d}\zeta$$

$$= -\frac{L}{2}F_y(t) + \sigma_{2y}v_{ry}\int_0^L f_n(\zeta)\zeta \mathrm{d}\zeta + \sigma_{0y}\sum_{k=0}^{m} c_k M^{0L}_{k+1,y} + \sigma_{1y}\sum_{k=0}^{m} c_k \dot{M}^{0L}_{k+1,y} \quad (16)$$

3.1 Closure Relationship

Equations (11), (12) require the time history of the internal friction states $z_i(t,\zeta)$ for fixed positions on the contact patch, namely, $\zeta = a$ and $\zeta = b$. In this section we discuss the calculation of these terms.

Going back to the original partial differential equation (1) let us consider the characteristics given by

$$t = t(s)\ , \quad \zeta = \zeta(s)$$

with

$$\frac{\partial t}{\partial s} = 1\ , \quad \frac{\partial \zeta}{\partial s} = |\omega r|.$$

Let the characteristic $y(s) = \zeta(t(s))$ starting from $\zeta = 0$ at time $t - \tau$ for some (still unknown) τ and ending at $\zeta = \zeta_0$ at time t. Then

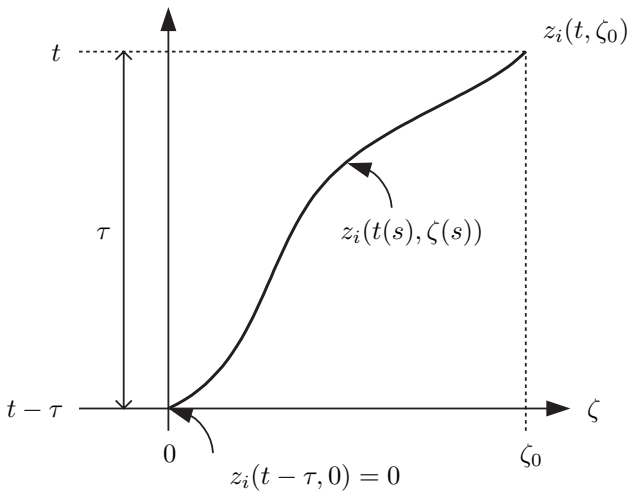

Figure 2: Solution $z_i(t,\zeta)$ along the characteristic $y(s) = \zeta(t(s))$.

$$y(t') = \int_{t-\tau}^{t'} |\omega r|(\sigma)\mathrm{d}\sigma \quad (17)$$

and $y(t) = \zeta_0$. Hence,

$$\zeta_0 \quad = \quad \int_{t-\tau}^{t} |\omega r|(\sigma)\mathrm{d}\sigma \tag{18}$$

Let us follow the solution along the characteristic (Fig. 2). To this end, define $\xi_i(t) := z_i(t, y(t))$. Thus,

$$\dot{\xi}_i(t) = \frac{\partial z_i}{\partial t} + \frac{\partial z_i}{\partial y}\frac{\partial y}{\partial t} = v_{ri} - C_{0i}(v_r)\xi_i(t) \tag{19}$$

with initial condition

$$\xi_i(t-\tau) = z_i(t-\tau, y(t-\tau)) = z_i(t-\tau, 0) = 0 \ .$$

Finally, $z_i(t, \zeta_0) = \xi_i(t)$ and τ is such that (18) holds. By setting $\zeta_0 = a$ and $\zeta_0 = b$ we now have an expression for the last term in (12).

4 THE EFFECT OF NORMAL FORCE DISTRIBUTION

In this section we derive the exact aggregate LuGre tire friction model for several specific cases of normal force distribution $f_n(\zeta)$. Namely, we provide the moment calculations for several simple load distributions commonly used in the literature (e.g., uniform, trapezoidal) [16, 6, 7, 8, 11, 12], as well as for the more realistic load distribution with quartic dependence. A quartic polynomial produces normal load profiles for f_n which are very close to empirical ones (Fig. 3(b)). At any rate, the methodology developed here may be used to incorporate any smooth or piecewise smooth $f_n(\zeta)$ load distribution along the patch. Figure 3(a) shows a comparison between several normal load distributions.

4.1 Exact Lumped Model for Uniform Load Distribution

The uniform load distribution $f_n(\zeta) = c_0$ is derived from (13) with $m = 0$ while in equations (11) and (12) we substitute $a = 0$ and $b = L$. The dynamics of friction are described by five ordinary differential equations with states $M_{0,x}^{0L}$, $M_{0,y}^{0L}$ from equation (12), $M_{1,y}^{0L}$ from equation (11) with $p = 1$ and $z_x(t, L)$, $z_y(t, L)$ from equation (19). A methodology for choosing appropriate initial conditions to integrate these ode's is discussed in Section 4.4.

4.2 Exact Lumped Model for Trapezoidal Load Distribution

In [11] it was shown that the LuGre tire friction model with uniform load distribution reproduced the longitudinal and lateral forces matching very well other empirical models (at least at steady-state). However, this model failed to reproduce realistic aligning torque characteristics. In order to accurately capture the behavior of the aligning moment one needs to introduce the effects of pneumatic

trail. This was achieved in [11] with the introduction of a trapezoidal normal load distribution (Fig. 3).

For a trapezoidal distribution the function $f_n(\zeta)$ is given by

$$f_n(\zeta) = \begin{cases} C_1\zeta & \text{for} \quad 0 \le \zeta \le a, \\ f_{\max} & \text{for} \quad a \le \zeta \le b, \\ C_2\zeta + C_3 & \text{for} \quad b \le \zeta \le L. \end{cases} \tag{20}$$

The normal load distribution above is only piecewise smooth and the approximation (13) cannot be used directly. In this case, it is necessary to consider different moments of $z_i(t,\zeta)$ for different parts of the contact patch. To this end let $M_{p,i}^{0a}(t)$ for $\zeta \in [0,\, a]$, $M_{p,i}^{ab}(t)$ for $\zeta \in (a,\, b)$ and $M_{p,i}^{bL}(t)$ for $\zeta \in [b,\, L]$. Thus, the dynamics of friction are described by a set of nineteen ordinary differential equations with states $z_i(t,a)$, $z_i(t,b)$ and $z_i(t,L)$, $M_{0,i}^{0a}$, $M_{0,i}^{ab}$ and $M_{0,i}^{bL}$ from equation (12), $M_{1,i}^{0a}$ and $M_{1,i}^{bL}$ from equation (11), with $i = x, y$ and finally $M_{2,y}^{0a}$, $M_{1,y}^{ab}$ and $M_{2,y}^{bL}$ again from equation (11). The calculation of $z_i(t,a)$, $z_i(t,b)$ and $z_i(t,L)$ is done in accordance to the discussion of Section 3.1 using equation (19). The choice of initial conditions is discussed in Section 4.4.

The forces are given by

$$\begin{aligned} F_i(t) \;=\; & -\sigma_{0i}\left(C_1 M_{1,i}^{0a} + f_{\max} M_{0,i}^{ab} + C_2 M_{1,i}^{bL} + C_3 M_{0,i}^{bL}\right) \\ & - \sigma_{1i}\left(C_1 \dot{M}_{1,i}^{0a} + f_{\max} \dot{M}_{0,i}^{ab} + C_2 \dot{M}_{1,i}^{bL} + C_3 \dot{M}_{0,i}^{bL}\right) \\ & - \sigma_{2i} v_{ri} F_n, \qquad i = x, y \end{aligned} \tag{21}$$

and the aligning torque by

$$\begin{aligned} M_z(t) = \; & - \; \frac{L}{2} F_y + \sigma_{2y} v_{ry} \int_0^L f_n(\zeta)\zeta \mathrm{d}\zeta \\ & + \; \sigma_{0y}\left(C_1 M_{2,y}^{0a} + f_{\max} M_{1,y}^{ab} + C_2 M_{2,y}^{bL} + C_3 M_{1,y}^{bL}\right) \\ & + \; \sigma_{1y}\left(C_1 \dot{M}_{2,y}^{0a} + f_{\max} \dot{M}_{1,y}^{ab} + C_2 \dot{M}_{2,y}^{bL} + C_3 \dot{M}_{1,y}^{bL}\right). \end{aligned} \tag{22}$$

4.3 Exact Lumped Model for a Quartic Load Distribution

In this section we introduce another approximation for the normal load distribution at the contact patch. The quartic normal load distribution (Fig. 3) is derived from (13) for $m = 4$:

$$f_n(\zeta) = c_4\zeta^4 + c_3\zeta^3 + c_2\zeta^2 + c_1\zeta + c_0 \tag{23}$$

Using this approximation, one is able to incorporate the effects of the pneumatic trail, resulting to realistic aligning torque predictions, as well as the natural boundary conditions of the normal load distribution, i.e. $f_n(\zeta = 0) = f_n(\zeta = L) = 0$. In addition, the proposed expression is smooth along the whole length of the contact patch and the pth moment of $z_i(t,\zeta)$ from $\zeta = 0$ to $\zeta = L$, $M_{p,i}^{0L}$, may be used. Thus, we avoid splitting the integral (10) as was done for the

trapezoidal distribution. This also results in a smaller number of states (and differential equations).

It can be easily shown that in this case the dynamics of the tire friction are described by a set of thirteen ordinary differential equations with states $z_x(t, L)$ and $z_y(t, L)$ from equation (19), $M_{p,x}^{0L}$ and $M_{p,y}^{0L}$ with $p = 0, 1, ..., 4$ from equations (11) and (12) and $M_{5,y}^{0L}$ from equation (11). Once again, the choice of initial conditions is discussed in Section 4.4.

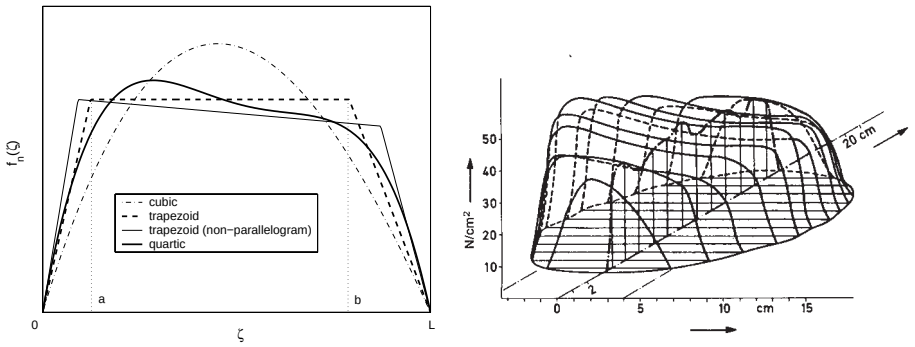

(a) (b)

Figure 3: (a) Possible choices of $f_n(\zeta)$; (b) Empirical plots of normal load distribution taken from [20].

4.4 Initial Conditions

The initial condition $\xi_i(0) = z_i(0, \zeta_0)$ required in (19) can be calculated easily by integrating (19) from $t = -\tau$ to $t = 0$, where

$$\tau = \frac{\zeta_0}{|\omega r|}. \tag{24}$$

Under the assumption that during this period v, ω and α are constant, one obtains

$$\xi(t = 0) = \frac{v_{ri}}{C_{0i}(v_r)} \left(1 - e^{-C_{0i}(v_r)\tau}\right) \tag{25}$$

Substituting τ from (24) in (25) one obtains

$$\xi(t = 0) = \frac{v_{ri}}{C_{0i}(v_r)} \left(1 - e^{-\frac{C_{0i}(v_r)\zeta_0}{|\omega r|}}\right) = z_i(0, \zeta_0) \tag{26}$$

The same result can also be obtained by assuming that the tire is initially at steady-state with constant ω, v and α. To this end, we may enforce $\frac{\partial z_i(t,\zeta)}{\partial t} = 0$ in equation (1) to obtain

$$\frac{\partial z_i(t, \zeta)}{\partial \zeta} = \frac{1}{|\omega r|} \Big(v_{ri} - C_{0i}(v_r) z_i(t, \zeta)\Big), \quad i = x, y \tag{27}$$

Taking into consideration the boundary condition $z_i(t,0) = 0$ (no deflection at the entry point of the contact patch) and the steady-state conditions of constant ω, v and α, we may integrate (27) to obtain the distribution $z_i^{ss}(\zeta)$ of z_i $(i = x, y)$, along the contact patch length at steady-state, as in [11] and [12].

$$z_i^{ss}(\zeta) = \frac{v_{ri}}{C_{0i}(v_r)} \left(1 - e^{-\frac{C_{0i}(v_r)\zeta}{|\omega r|}}\right) \ , \quad i = x, y \tag{28}$$

Note that for $\zeta = \zeta_0$ the previous expression coincides with (26).

Using the expression (28), equivalently (26), in (9) we can then calculate the initial conditions $M_{pi}^{ab}(0)$ for all the moment equations (11), (12).

5 NUMERICAL SIMULATIONS

In this section we present numerical simulations of the previously developed lumped LuGre tire friction models [10, 11, 12] and compare the results with the exact lumped model developed in this paper. The tire friction models under consideration are subject to the same excitation, consisting of a linearly decreasing angular rate ω from 32 rad/sec to zero within 2 sec, and constant velocity v and slip angle α (Fig. 1). It should be pointed out that this is a controlled excitation that can be achieved only in a laboratory environment. For a wheeled vehicle, reduction in ω is normally accompanied by a reduction in the vehicle speed v as well.

5.1 Uniform Normal Load Distribution

In [11] two approximate lumped LuGre tire friction models were developed. These models are summarized in the equations below:

$$\dot{\tilde{z}}_i(t) = v_{ri} - \left(C_{0i}(v_r) + \frac{\kappa_i}{L}|\omega r|\right) \tilde{z}_i(t), \quad i = x, y \tag{29}$$

$$F_i(t) = -F_n \left(\sigma_{0i}\tilde{z}_i + \sigma_{1i}\dot{\tilde{z}}_i + \sigma_{2i}v_{ri}\right), \quad i = x, y \tag{30}$$

The two different lumped models correspond to different choices (approximations) of κ_i. This term is either approximated as constant, i.e., $\kappa_i \in [1.1 \ \ 1.4]$, or as a function of ω and v_r, i.e., $\kappa_i = \kappa_i^{ss}(v_r, \omega)$, such that the steady-state solution of the lumped model captures exactly the *steady-state* solution of the distributed model. In the latter case the expression for κ_i is given as follows [11]

$$\kappa_i^{ss} = \frac{1 - e^{-L/Z_i}}{1 - \frac{Z_i}{L}\left(1 - e^{-L/Z_i}\right)} \ , \quad Z_i = \frac{|\omega r|}{C_{0i}(v_r)} \tag{31}$$

It is shown in [11] that the approximate lumped model captures the steady-state characteristics of the distributed friction very well, while no guarantees for the accuracy of the model during transient were available. Evaluation of the effect

of these transients is now possible via comparison with the exact lumped model presented in Section 4.1.

Two cases are investigated in this section. The first case assumes low tire stiffness ($\sigma_{0i} = 150$ m^{-1}, $i = x, y$) while the second case assumes a higher tire stiffness ($\sigma_{0i} = 500$ m^{-1}, $i = x, y$). The time histories of the friction forces (Fig. 4) show that the approximations for κ_i made in [11] are more realistic when the stiffness of the tire is higher. In this case the steady-state is reached faster. As already mentioned, the approximate lumped models in [11, 12] were derived having only the accuracy of the steady-state behavior in mind.

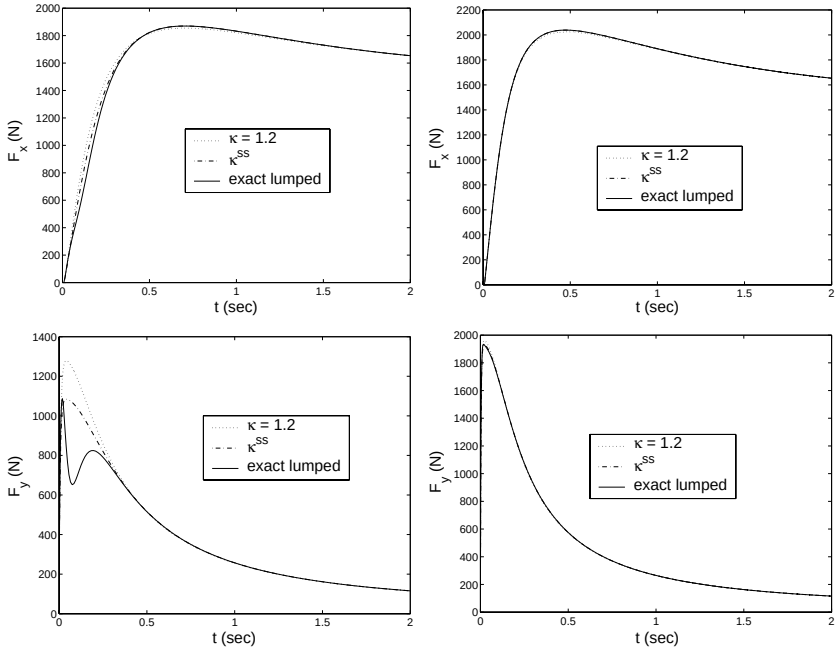

Figure 4: Time histories for longitudinal and lateral forces for uniform load distribution (left column: $\sigma_{0i} = 150$ m^{-1}, right column: $\sigma_{0i} = 500$ m^{-1}, $i = x, y$)

5.2 Trapezoidal and Quartic Load Distribution

In [12] an approximate average lumped model was developed for the case of the trapezoidal normal load distribution. The dynamics of the friction forces are given by (29) and (30). In [12] the term κ_i was approximated by κ_i^{ss} such that the force prediction of the lumped model matches the one from the distributed model at steady-state. The aligning torque predictions of the LuGre tire friction model with a trapezoidal normal load distribution are comparable to experimental data [11], [12]. The dynamics of the aligning torque that completes the approximate average lumped model in [11], [12] are summarized

below:

$$\dot{\hat{z}}_y(t) = \frac{G}{F_n L} v_{ry} - C_{0y}\hat{z}_y(t) - \nu(t)|\omega r|\hat{z}_y(t) + \frac{|\omega r|}{L}\bar{z}_y(t) \quad (32)$$

$$M_z(t) = F_n L\left[\sigma_{0y}\left(\frac{1}{2}\tilde{z}_y - \hat{z}_y\right) + \sigma_{1y}\left(\frac{1}{2}\dot{\tilde{z}}_y - \dot{\hat{z}}_y\right) + \sigma_{2y}\left(\frac{1}{2}v_{ry} - \frac{G}{F_n L}\right)\right] \quad (33)$$

where

$$G = \int_0^L f_n(\zeta)\zeta \mathrm{d}\zeta$$

Similarly to the approximation of the κ_i term for the friction forces, the $\nu(t)$ term in (32) was approximated in [12] by a function ν^{ss}, such that the aligning torque predictions of the average lumped and the distributed model agree at steady-state.

Next, we compare the dynamic behavior of the average lumped model developed in [12] with the behavior of the model presented in Sections 4.2 and 4.3. In order to make a fair comparison between the trapezoidal and the quartic normal load distribution models we have selected the parameters of the two expressions (20) and (23) such that they produce the same total normal force F_n and the same pneumatic trail.

We consider the case of a tire with stiffness $\sigma_{0i} = 500\ \mathrm{m}^{-1},\ i = x, y$. The excitation of the system remains the same as before. The results are shown on the left column of Fig. 5. In Fig. 5 the time histories of the friction forces and the aligning torque are shown. We observe that the three models converge to the same steady-state, as expected. However, significant differences in the transient behavior of the three models are also evident. These differences are more apparent in the lateral force F_y and aligning torque M_z. The discrepancy is due to the fact that the normal load distribution $f_n(\zeta)$, along with the distribution of the contact patch deflection $z_i(t,\zeta)$, determine the amount of the total friction generated by each tire element along the contact patch length (see equations (2), (3)) at each time t. In the case of the approximate lumped model of [12] the use of the states $\tilde{z}_i(t),\ i = x, y$ and $\hat{z}_y(t)$ averages out the individual contribution to the total friction of each tire element, thus resulting in smoother transient behavior of the friction forces and aligning torque. In the case of the exact lumped model on the other hand, the product of the individual contact patch deflection $z_i(t,\zeta)$ with $f_n(\zeta)$ determines the amount of friction generated by each tire element in the contact patch; see equations (2)-(3). This is true both for the distributed and the exact lumped models. In Fig. 3(a) one observes that the trapezoidal normal load distribution weights more the tire elements close to the entry point of the contact patch (especially in the area $\zeta < a$) when compared to the quartic distribution. Similarly, the quartic distribution places more emphasis than the trapezoidal on the part of the patch $\zeta > a$. Observing the initial distribution of z_y^{ss} in Fig. 6 we notice that the tire elements close to $\zeta = 0$ are less deformed compared to the tire

elements for larger values of ζ. As a result, the quartic distribution gives higher values for F_y than the trapezoidal distribution at the initial time. As the time progresses, and ω is reduced, (for example, $\omega = 20$ rad/sec) the distribution of z_y^{ss} tends to a uniform one. Since the total normal load is the same for both the quartic and the trapezoidal distributions, the two distributions will give similar values after the transients have receded. This is verified from the results shown in Fig. 5.

To provide an additional confirmation of these observations, a second set of numerical simulations was performed, using the approximate model in [12] and the exact trapezoidal and quartic models of Sections 4.2, 4.3 respectively, but with a larger slip angle, namely $\alpha = 15^\circ$. The tire stiffness and the excitation remained the same. The results are shown in the right column of Fig. 5. For this case the time histories of the friction forces and the aligning moment are almost identical for all three cases of normal load distributions. The right plot in Fig. 6 reveals that for $\alpha = 15^\circ$ the distribution of z_y^{ss} is very close to a uniform one, thus corroborating the earlier observations.

6 CONCLUSIONS

A methodology to compute the exact dynamics of the aggregate distributed LuGre dynamic tire friction model by a set of ordinary differential equations is presented. The results of this work allow one to test/validate the assumptions introduced in the development of other low-order approximate lumped models. A comparative analysis shows that, given a sufficiently high stiffness of the tire, the approximate models reproduce the dynamics of the aggregate distributed tire model very accurately.

REFERENCES

1. Bliman P. and Sorine M.: A system-theoretic approach of systems with hysteresis application to friction modelling and compensation. In *Proceedings of 2nd European Control Conference*, (Gröningen, The Netherlands), 1993.
2. Bliman P. and Sorine M.: Easy-to-use realistic dry friction models for automatic control. In *Proceedings of 3rd European Control Conference*, (Rome, Italy), pp. 3788–3794, September 1995.
3. Bliman P., Bonald T., and Sorine M.: Hysteresis operators and tyre friction models. Application to vehicle dynamic simulation. In *Proceedings of ICIAM 95*, (Hamburg, Germany), July 3-7 1995.
4. Sorine M. and Szymanski J.: A new dynamic multi d.o.f. tire model. In *Transportation Systems 2000*, (Braunschweig, Germany), 2000.
5. Szymanski J.: Modèles réduits du contact pneu-sol et applications à l'automobile. Technical Report, Renault, Technocentre Renault, Guyancourt, France, 1999.
6. Canudas de Wit C. and Tsiotras P.: Dynamic tire friction models for vehicle traction control. In *Proceedings of 38th IEEE Conference on Decision and Control*, (Phoenix, Arizona, USA), pp. 3746–3751, 1999.

7. Deur J.: Modeling and analysis of longitudinal tire dynamics based on the LuGre friction model. Technical Report, Ford Motor Company, Scientific Research Laboratory MD 1170, Dearborn, MI 48121-2053, USA, 2001.
8. Canudas de Wit C., Tsiotras P., Velenis E., Basset M. and Gissinger G.: Dynamic friction models for road/tire longitudinal interaction. *Vehicle System Dynamics*, vol. 39, no. 3, pp. 189–226, 2003.
9. Canudas de Wit C., Olsson H., Åström K. J. and Lischinsky P.: A new model for control of systems with friction. *IEEE Transactions on Automatic Control*, vol. 40, no. 3, pp. 419–425, 1995.
10. Claeys X., Canudas de Wit C., Yi J., Horowitz R., Alvarez L. and Richard L.: A new 3d dynamic tire/road friction model for vehicle simulation and control. In *Proceedings of the ASME-IMECE World Conference*, (New York, USA), November 2001.
11. Deur J., Asgari J. and Hrovat D.: A dynamic tire friction model for combined longitudinal and lateral motion. In *Proceedings of the ASME-IMECE World Conference*, (New York, USA), November 2001.
12. Velenis E., Tsiotras P. and Canudas-de Wit C.: Extension of the lugre dynamic tire friction model to 2d motion. In *Proceedings of the 10th IEEE Mediterranean Conference on Control and Automation - MED2002*, July 9-12 2002. Lisbon, Portugal.
13. Sorine M.: Applications of hysteresis models: Contact friction in tires, muscle contraction. In *IEEE CDC 98 Workshop #2*, (Tampa, Florida), 1998.
14. Canudas-de Wit C., Petersen M. and Shiriaev A.: A new nonlinear observer for tire/road distributed contact friction. In *Proceedings of the* 42^{th} *IEEE Conference on Decision and Control*, December 9-12 2003. Maui, Hawaii.
15. Canudas de Wit C., Horowitz R. and Tsiotras P.: Model-based observers for tire/road contact friction prediction. In *New Directions in Nonlinear Observer Design* (H. Nijmeijer and T. Fossen, eds.), vol. 244 of *Lecture Notes in Control and Information Science*, pp. 23–42, London: Springer-Verlag, 1999.
16. Yamazaki S., Furukawa O. and Suzuki T.: Study on real time estimation of tire to road friction. *Vehicle System Dynamics*, vol. 27, pp. 225–233, 1999.
17. Akhiezer N.: *The Classical Moment Problem.* Hafner Publishing Company, New York, 1965.
18. Moore J. and Pizer R.: *Moment Methods in Electromagnetics.* Research Studies Press LTD, Letchworth, Hertfordshire, England, 1986.
19. Zahalak G.: A comparison of the mechanical behavior of the cat soleus muscle with a distribution-moment model. *Transactions of the ASME Journal of Biomechanical Engineering*, vol. 108, pp. 131–140, 1986.
20. Zomotor A.: *Fahrwerktechnik: Fahrverhalten.* Vogel Buchverlag Würzburg, 1987.

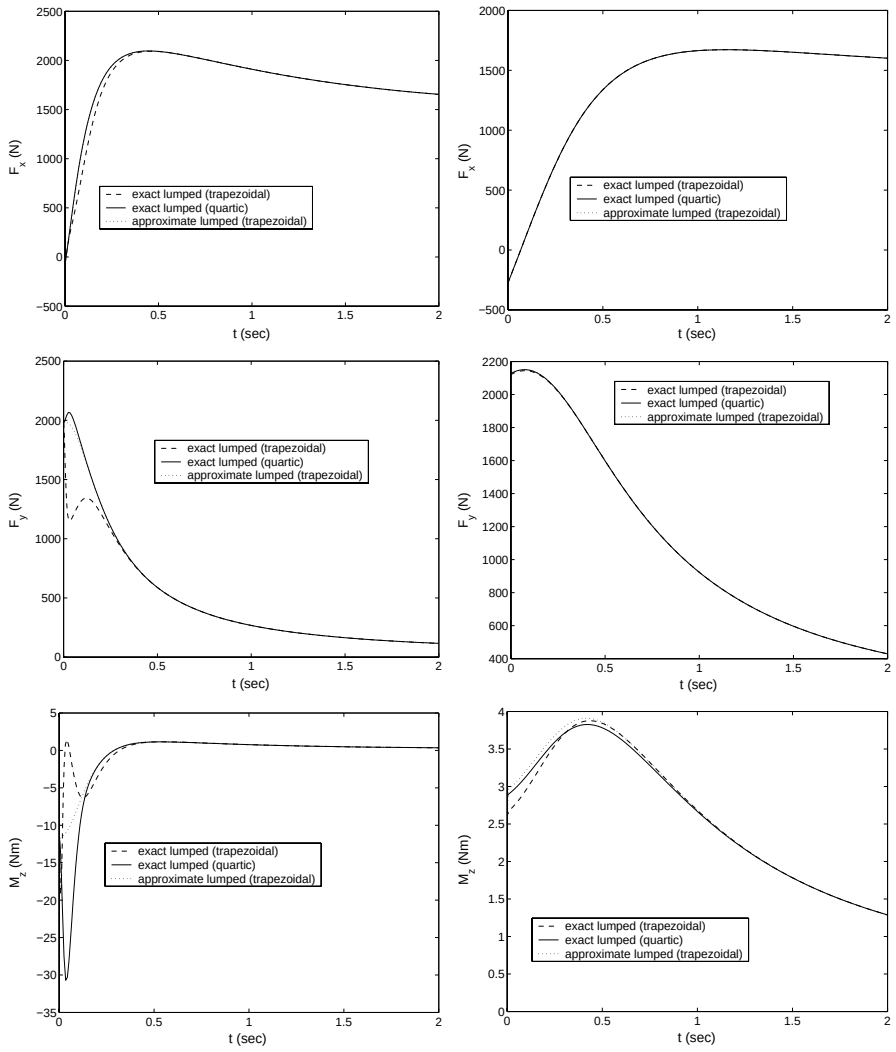

Figure 5: Time histories for longitudinal/lateral forces and aligning torque (trapezoidal and quartic normal load distribution), left column: $\alpha = 4°$, right column: $\alpha = 15°$

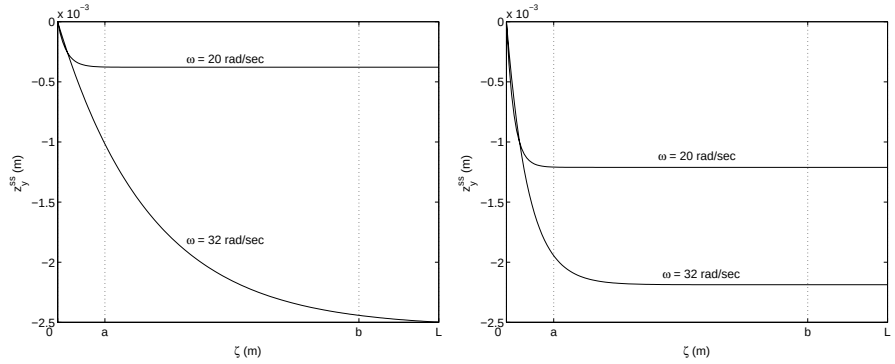

Figure 6: Distribution of $z_y^{ss}(\zeta)$ along the contact patch, left column: $\alpha = 4^\circ$, right column: $\alpha = 15^\circ$